Supplementary Information

Measurement-based modeling of daytime and nighttime oxidation of atmospheric mercury

Maor Gabay, Mordechai Peleg, Erick Fredj, Eran Tas

Accurate characterization of gaseous elemental mercury (GEM) chemical oxidation pathways and their kinetics is critically important for assessing the transfer of atmospheric mercury to bioaquatic systems. Recent comprehensive field measurements have suggested a role for the nitrate radical (NO_3) in efficient nighttime oxidation of GEM, and underestimation of the role of the hydroxyl radical (OH) as a GEM oxidant. We used the CAABA/MECCA chemical box model and measurement-based kinetic calculations to analyze these measurement results, in order to investigate the nighttime and daytime oxidation of GEM. We assumed a second-order reaction for the NO_3-induced nighttime oxidation of GEM. Our analysis demonstrates that nighttime oxidation of GEM has to be included in the model to account for the measured variations in nighttime RGM concentration. A lower limit and best-fit rate constant for the GEM nighttime oxidation are provided. To the best of our knowledge, this is the first time that a rate for the nighttime oxidation of GEM has been determined based on field measurements. Our analysis further indicates that OH has a much more important role in GEM oxidation than commonly considered. A lower-limit rate constant for the OH–RGM reaction is provided.

The following presents the way in which the rate constants $k[OH+Hg^0]$ and $k[NO_3+Hg^0]$ were calculated (Sect. S1) and a tabulated summary of the mercury chemical mechanism used by the CAABA/MECCA (Sect. S2).

S1. Rate constant calculations

The field measurements were used to estimate the rate constants for GEM oxidation by O_3 and OH. It should be emphasized that the estimations are based only on gas-phase kinetic calculations, such that their accuracy depends on the extent of aerosol activity

and additional removal and recycling processes occurring during the measurements. Considering the fact that measured fine particulate-bound mercury (FPM) concentrations were relatively low in the studied area, the aerosol activity appears to be relatively low. This may be the result of the low RH in the area. Nevertheless, our analyses indicated that RGM-removal processes are underestimated in our model, particularly during the night, implying underestimation of the calculated rate constants.

The kinetic calculations were based on 27 selected measurement days which showed a definite daytime RGM peak and no corresponding sharp RH decrease (which might lead to a shift in the gas–aerosol partitioning). Since OH concentrations were not available for the measurement site, a theoretical diurnal OH profile was constructed for the respective days (Fig. 1 in the paper). The construction was based on the assumptions that the OH concentration is predominantly correlated with UV intensity, and that maximal OH concentration is 0.5 ppt, based on a review by Stone et al. (2012) who compared spring and summer measurements in semi-polluted regions located between 53° and 39° N. This value was close to the highest level of OH mentioned in Stone et al. (2012). A relatively high concentration was chosen due to the strong radiation and high ozone level in Jerusalem, which contribute to OH formation; 0.5 ppt OH is a reasonable level, even for polluted regions (Stone et al., 2012), and we therefore believe that the calculated rate constant k[OH+Hg^0] can be considered a lower rate limit, from this aspect. Moreover, note that the CAABA/MECCA model calculated lower OH concentrations: 0.2 and 0.3 ppt for 83 and 120 ppb ozone, respectively. A theoretical diurnal profile for OH was then constructed for 7 Jul 2012, based on the assumption that the OH concentration is correlated with UV intensity (Smith et al., 2006; von Glasow et al., 2002). Data were taken from a nearby weather station (Nayot, Jerusalem). The timing of the maximal OH concentration was set to the known maximal radiation time.

The oxidation rate of Hg^0 by OH was estimated based on the daily peak in RGM and OH concentrations at around noon, assuming that the rate is only dependent on O_3, OH and GEM concentrations, as described in Eq. (S1):

$$\frac{\Delta[RGM]}{\Delta t} = k_{[O_3]} \cdot [O_3] \cdot [GEM] + k_{[OH]} \cdot [OH] \cdot [GEM] \quad \text{(S1)}$$

Therefore, the rate constant of oxidation by OH alone can be described by:

$$k_{[OH+Hg^0]}\ \ (cm^3 molec^{-1} sec^{-1}) = \frac{\frac{\Delta[RGM]}{\Delta t \cdot [GEM]} - k_{[O_3+Hg]} \cdot [O_3]}{[OH]} \qquad \text{(S2)}$$

where Δ[RGM] is the measured daytime RGM peak for the 27 selected days (measured as the difference between peak and baseline RGM concentrations), Δt is the peak duration time (from the elevated RGM formation at around noon to maximum RGM concentrations), [GEM] is the average measured GEM concentration (210 ppq), [OH] is the constructed OH concentration during the RGM peak, [O_3] is the O_3 concentration measured concurrent with the RGM peak, and k[O_3+Hg^0] is the rate constant of oxidation of Hg^0 by O_3 (the value of k[O_3+Hg^0] is taken as 3.11E-20 or 7.5E-19 cm^3 $molecule^{-1}$ s^{-1} with respect to the simulation scenario; see Table 1). Note that k[OH+Hg^0] in Eq. S2 represents a lower limit value for the oxidation rate of GEM by OH, because the equation does not include RGM-removal processes, as explained above. When k[O_3+Hg^0] = 3.11E-20 cm^3 $molecule^{-1}$ s^{-1} (Hall, 1995) is used, $k[OH + Hg^0]$=2.8 (±0.5)E-13 cm^3 $molecule^{-1}$ s^{-1}, and when using k[O_3+Hg^0] = 7.5E-19 cm^3 $molecule^{-1}$ s^{-1} (Pal and Ariya, 2004b), $k[OH + Hg^0]$=1.1 (±0.5) E-13 cm^3 $molecule^{-1}$ s^{-1}. The errors mentioned here represent the standard deviations of the mean.

The nighttime oxidation rate constant of GEM by NO_3 was estimated based on the concurrent nighttime peaks in RGM and NO_3 observed during the measurement campaign, using Eq. (S3):

$$k_{[NO_3+Hg^0]}\ \ (cm^3 molec^{-1} sec^{-1}) = \frac{\frac{\Delta[RGM]}{\Delta t \cdot [GEM]} - k_{[O_3+Hg]} \cdot [O_3]}{[NO_3]} \qquad \text{(S3)}$$

Δ[RGM] represents the nighttime RGM peak (measured as the difference in RGM concentration between peak maximum and minimum) over the 19 measurement days for which a distinct peak in RGM concentration could be identified during the night. [NO_3] and [O_3] are the measured NO_3 and O_3 concentrations corresponding to Δ[RGM]. Δt is the time duration of the peaks for which Δ[RGM] was calculated. k[O_3+Hg^0] is taken as 3.11E-20 or 7.5E-19 cm^3 $molecule^{-1}$ s^{-1} based on our simulation scenarios (see Table 1 and Sect. 3.2 in the paper). Note that Eq. S3 assumes a second-order rate

constant dependency on GEM and NO_3 as explained above. Note further that $k[NO_3+Hg^0]$ in Eq. S3 represents a lower limit value for the nighttime oxidation rate of GEM, because the equation does not include RGM-removal processes, which in reality probably affect RGM, as explained above. When $k[O_3+Hg^0]$ = 3.11E-20 cm^3 $molecule^{-1}$ s^{-1} (Hall, 1995) is used, $k[NO_3 + Hg^0]$=2.8 (±0.5)E-15 cm^3 $molecule^{-1}$ s^{-1}, and when $k[O_3+Hg^0]$ = 7.5E-19 cm^3 $molecule^{-1}$ s^{-1} (Pal and Ariya, 2004b) is used, $k[NO_3 + Hg^0]$=1.9E(±0.5)-15 $cm^3 molecule^{-1} s^{-1}$. The errors mentioned here represent the standard deviations of the mean.

S2. Oxidation pathways of mercury used for the BASE simulation

Table S1. Gas-phase reactions.

Reaction		k [cm^3 $molecule^{-1}$ s^{-1}] or s^{-1}	
G1	$Hg+O_3 \rightarrow HgO+O_2$	$2.11E-18\times\exp(-1256.5K/T)$*	a
G2	$Hg+OH \rightarrow HgO+H$	$3.55E-14\times\exp(294K/T)$	b
G3	$Hg+NO_3 \rightarrow HgO+NO_2$	$4.0E-15$	c
G4	$Hg + Br \rightarrow HgBr$	$3.0E-13$	d
G6	$HgBr + BrO \rightarrow BrHgOBr$	$3.0E-12$	e
G7	$Hg + BrO \rightarrow HgO + Br$	$1.0E-13$	d
G8	$Hg+H_2O_2 \rightarrow HgO+H_2O$	$8.5E-19$	f
G10	$Hg + Br_2 \rightarrow HgBr_2$	$9.0E-17$	g
G11	$HgBr + Br \rightarrow HgBr_2$	$3.0E-12$	h
G12	$HgBr+Cl \rightarrow ClHgBr$	$3.0E-12$	h
G13	$HgCl+Br \rightarrow ClHgBr$	$3.0E-12$	h
G14	$Hg + Cl \rightarrow HgCl$	$1.0E-11$	g
G15	$Hg + Cl_2 \rightarrow HgCl_2$	$2.6E-18$	g

* A value of $8.43E-17\times\exp(-1407K/T)$ (Pal and Ariya, 2004b) was used for the PAL-ARIYA simulation; [a]Hall (1995); [b]Pal and Ariya (2004a); [c]Sommar et al. (1997); [d]Xie et al. (2008); [e]Shon et al. (2005); [f]Tokos et al. (1998); [g]Ariya et al. (2002); [h]Calvert and Lindberg (2003).

Table S2. Aqueous-phase reactions.

Reaction		K [$M^{-1}s^{-1}$] or s^{-1}	
A1	$Hg+O_3 \rightarrow HgO+O_2$	$4.7E7$	a
A2	$HgO+H^+ \rightarrow Hg^{2+}+OH^-$	$1.0E10$	b
A3	$Hg+OH \rightarrow Hg^{+}+OH^-$	$2.0E9$	c
A4	$Hg^{+}+OH \rightarrow Hg^{++}+OH^-$	$1.0E10$	c
A5	$Hg^{2+}+HO_2 \rightarrow Hg^{+}+O_2+H^+$	$1.7E4$	d
A6	$Hg^{+}+HO_2 \rightarrow Hg+O_2+H^+$	$1.0E10$	e
A7	$Hg+HOCl \rightarrow Hg^{2+}+Cl^-+OH^-$	$2.09E6$	f
A8	$Hg+ClO^- +H^+ \rightarrow Hg^{2+}+Cl^-+OH^-$	$1.99E6$	f
A9	$Hg+HOBr^- \rightarrow Hg_2^{+}+Br^-+OH^-$	0.279	g
A11	$Hg+Br_2 \rightarrow Hg^{2+}+2Br^-$	0.196	g
A12	$HgSO_3+H2O \rightarrow Hg+HSO_4^- +H^+$	0.0106	h

[a]Munthe (1992); [b]Pleuel and Munthe (1995); [c]Lin and Pehkonen (1997); [d]Pehkonen and Lin (1998); [e]Xie et al. (2008); [f]Lin and Pehkonen (1999); [g]Wang and Pehkonen (2004); [h]Van Loon et al. (2000).

Table S3. Henry's Law coefficient K_H.

Reaction		K_H [M atm^{-1}]	
H1	$Hg \leftrightarrow Hg_{(aq)}$	0.13	a
H2	$HgO_{(g)} \leftrightarrow HgO_{(aq)}$	$3.2E6$	b
H3	$HgCl_2 \leftrightarrow HgCl2(aq)$	$2.4E7$	b
H4	$HgBr_2 \leftrightarrow HgBr_2(aq)$	$2.4E7$	c
H5	$ClHgBr \leftrightarrow ClHgBr_{(aq)}$	$2.4E7$	c
H6	$BrHgOBr \leftrightarrow BrHgOBr_{(aq)}$	$2.4E7$	c
H7	$ClHgOBr \leftrightarrow ClHgOBr_{(aq)}$	$2.4E7$	c

[a]As cited by Schroeder and Munthe (1998); [b]As cited by Shon et al. (2005). [c]Xie et al. (2008).

Table S4. Aqueous-phase equilibria.

Reaction		K [M^{-1}]	
EQ1	$Hg(II)+OH^- \leftrightarrow Hg(OH)^+$	$4E10$	a
EQ2	$Hg(OH)^+ + OH^- \leftrightarrow Hg(OH)_2$	$1.6E11$	a
EQ3	$Hg^{2+} + SO_3^{2-} \leftrightarrow HgSO_3$	$2E13$	b
EQ4	$HgSO_3 + SO_3^{2-} \leftrightarrow Hg(SO_3)2^{2-}$	$1E10$	b
EQ5	$Hg(OH)^+ + Cl^- \leftrightarrow HgOHCl$	$2.7E7$	a
EQ6	$Hg(II)+Cl^- \leftrightarrow HgCl^+$	$5.8E6$	c
EQ7	$HgCl^+ + Cl^- \leftrightarrow HgCl_2$	$2.5E6$	c
EQ8	$HgCl_2 + Cl^- \leftrightarrow HgCl_3^-$	6.7	c
EQ9	$HgCl_3^- + Cl^- \leftrightarrow HgCl_4^{2-}$	$1.3E1$	c
EQ10	$Hg(II)+Br^- \leftrightarrow HgBr^+$	$1.1E9$	c
EQ11	$HgBr^+ + Br^- \leftrightarrow HgBr_2$	$2.5E8$	c
EQ12	$HgBr_2 + Br^- \leftrightarrow HgBr_3^-$	$1.5E2$	c
EQ13	$HgBr_3^- + Br^- \leftrightarrow HgBr_4^{2-}$	$2.3E1$	c

[a]Pleuel and Munthe (1995); [b]Van Loon et al. (2001); [c]Hepler and Olofsson (1975).

S3. FIT set of simulations

Table 5 summarizes the results obtained with the FIT set of simulations (see Sect. 2.2 in the paper). Use of Pal and Ariya (2004b) or Hall (1995) k[O_3+Hg^0] values combined with adjusted k[NO_3+Hg^0] (to provide best fit with the measured RGM) and k[OH+Hg^0] = 6.50E-13 cm^3 $molecule^{-1}$ s^{-1} resulted in a relatively small delay in the HgO peak with respect to the compatible measured noontime RGM peak. Applying Sommar et al.'s (2001) k[OH+Hg^0] value with adjusted k[O_3+Hg^0] and k[NO_3+Hg^0] resulted in a much larger delay (>3 h), indicating that Sommar et al. (2001) significantly underestimated k[OH+Hg^0] (Fig. S1). Furthermore, due to the relatively high k[O_3+Hg^0], the HgO peak obtained by this simulation was much more shallow and extended much further. Hence, the analysis presented in this section further indicates that reasonable reproduction of the measured RGM can only be achieved by significantly reducing the commonly used k[O_3+Hg^0] with respect to k[OH+Hg^0].

Table S5. Summary of the results of the FIT set of simulations. References are provided where the used rate constant was adapted from the literature.

k[O_3+Hg^0] cm^3 $molecule^{-1}$ s^{-1}	k[OH+Hg^0] cm^3 $molecule^{-1}$ s^{-1}	k[NO_3+Hg^0] cm^3 $molecule^{-1}$ s^{-1}	HgO peak timing with respect to the measurements (delay in hours)
3.11E-20[a]	9.00E-13	2.30E-15	~0.5
7.50E-19[b]	6.50E-13	1.60E-15	~0.5
1.80E-18	9.52E-14[c]	1.50E-16	>3

[a]Hall (1995); [b]Pal and Ariya (2004b); [c]Sommar et al. (2001).

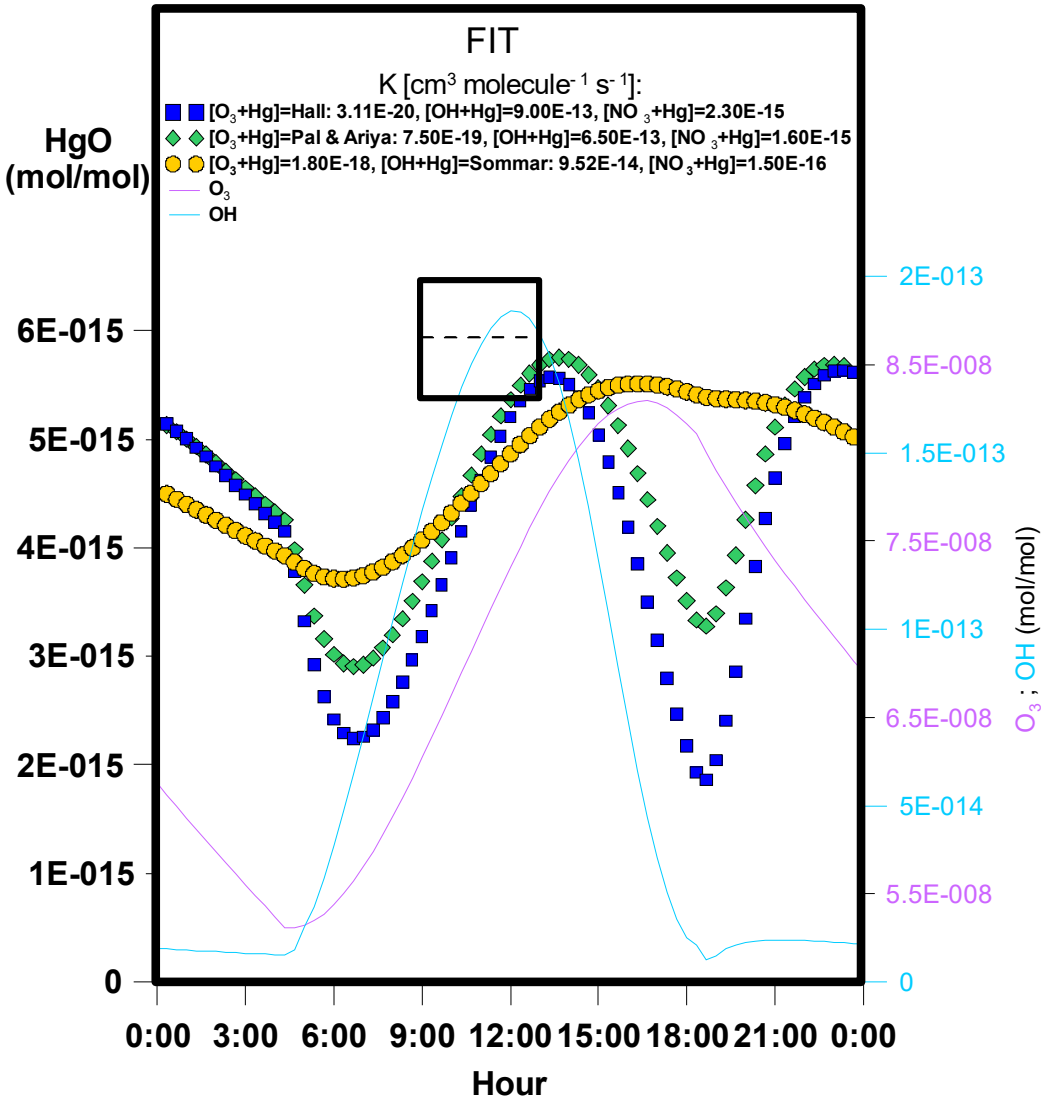

Figure S1. Dependency of HgO diurnal profile on oxidation by OH and O_3. The figure shows the HgO concentration obtained using the FIT set of simulations (Sect. 2.2 in the paper). The used $k[O_3+Hg^0]$, $k[OH+Hg^0]$ and $k[NO_3+Hg^0]$ values and simulated O_3 and OH concentrations are also presented. The dashed line inside the box indicates the average measured RGM maximum during the day (5.88 ppq; see Fig. 3 in the paper) and the time during which the maxima occurred (~0900–1300 h; see Fig. 1 in the paper). The vertical dimension of the box marks the corresponding standard deviation of the mean (0.53 ppq) of the measured daytime RGM maxima.

S4. DRYDEP set of simulations

Figure S2 presents the diurnal HgO profile obtained using the DRYDEP set of simulations, which are similar to BASE, but use different dry deposition velocities (Table 1 in the paper). Note that BASE uses a dry deposition of 0.5 cm s^{-1}, which was used by Mason and Sheu (2002) for the marine boundary layer. Typical HgO dry deposition in suburban areas might be higher. For instance, a deposition velocity of 1.52 ± 0.58, in addition to 0.03 ± 0.02 cm s^{-1}, has been reported for suburban areas (e.g., Zhang et al., 2009). According to DRYDEP sensitivity analysis, the difference in simulated HgO, when increasing deposition velocity from 0.5 cm s^{-1} to 2 cm s^{-1} and 5 cm s^{-1}, ranges from 1.52E-17–5.45E-17 mol mol^{-1} and 3.84E-17–1.42E-16 mol mol^{-1}, respectively. The average simulated HgO concentration decreased by 8.6% and 22%, and the maximal simulated daily HgO concentration decreased by 7.5% and 19.5%, when increasing deposition velocity from 0.5 cm s^{-1} to 2 cm s^{-1} and 5 cm s^{-1}, respectively (see Fig. S2).

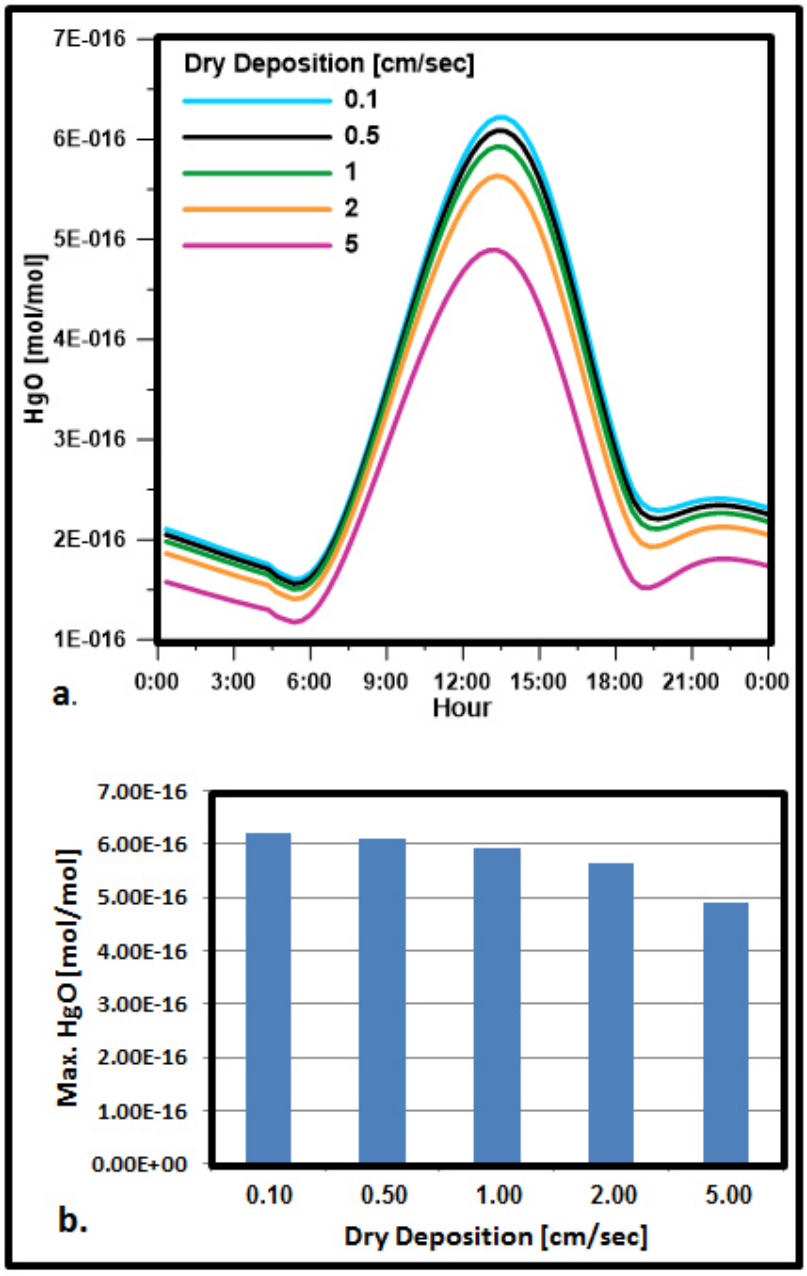

Figure S2. Impact of dry deposition on HgO concentrations. (**a**) Diurnal HgO profile obtained using the DRYDEP set of simulations (Sect. 2.2 in the paper). (**b**) Maximal HgO concentration obtained using the DRYDEP set of simulations shown in panel (a).

S5. Comparison between field measurements and model results for major GEM oxidants

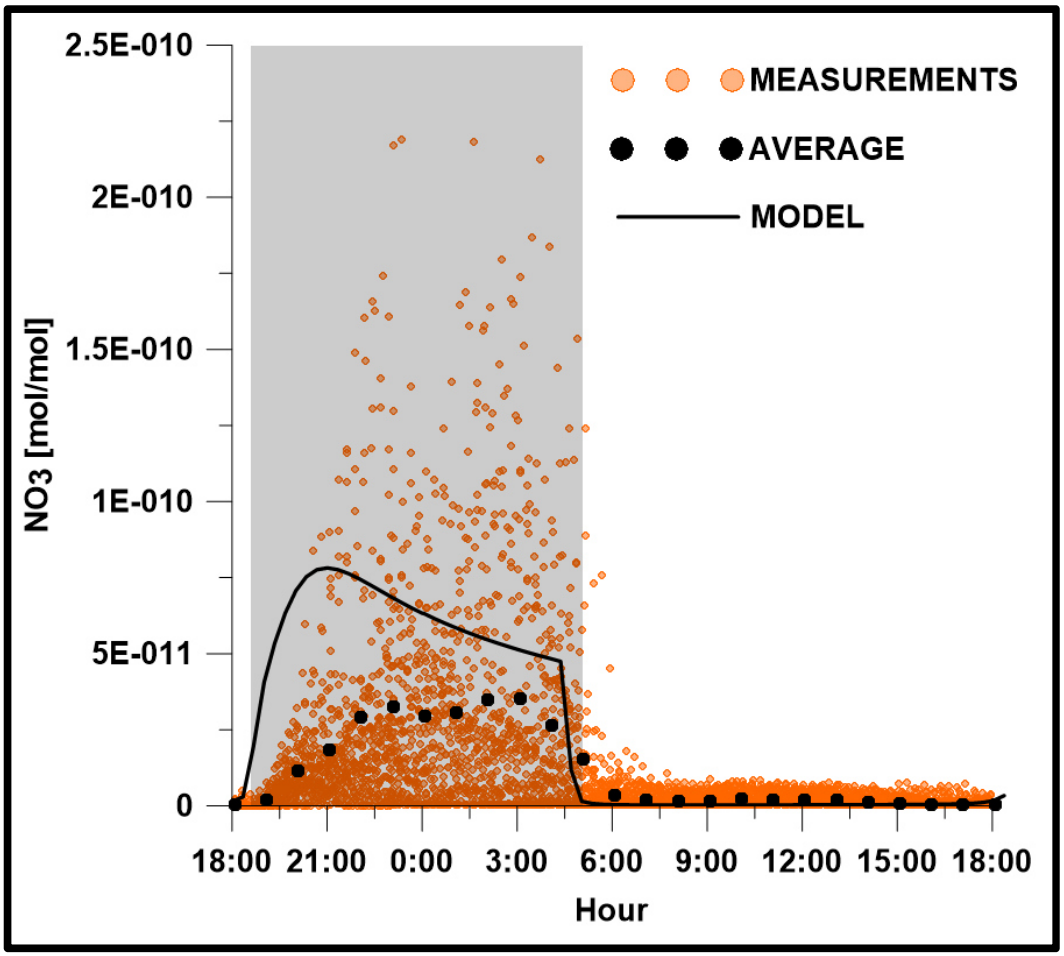

Figure S3. Comparison between measured (orange dots) and simulated (black line) diurnal NO_3 profiles. The black dots mark the average measured diurnal NO_3 profile. The shaded area represents nighttime.

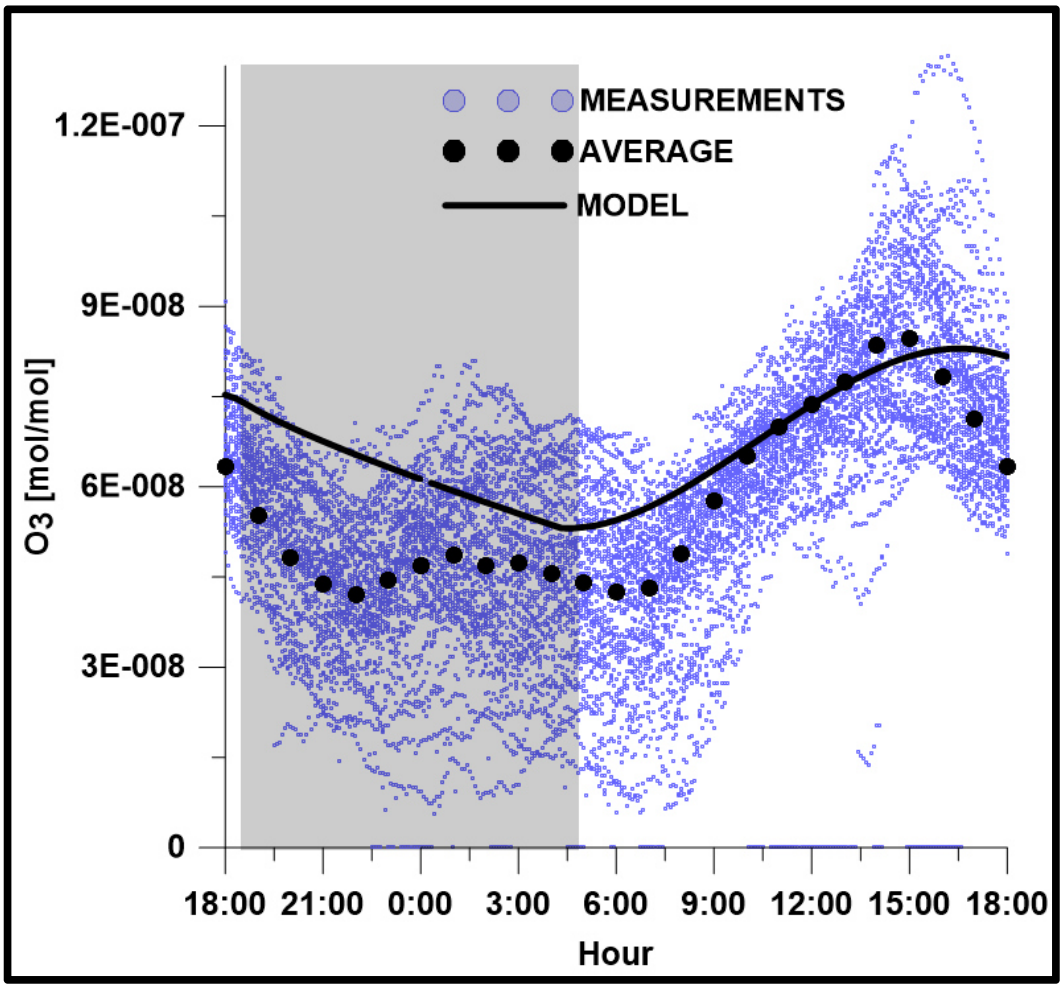

Figure S4. Comparison between measured (blue dots) and simulated (black line) diurnal O_3 profiles. The black dots mark the average measured diurnal O_3 profile. The shaded area represents nighttime.

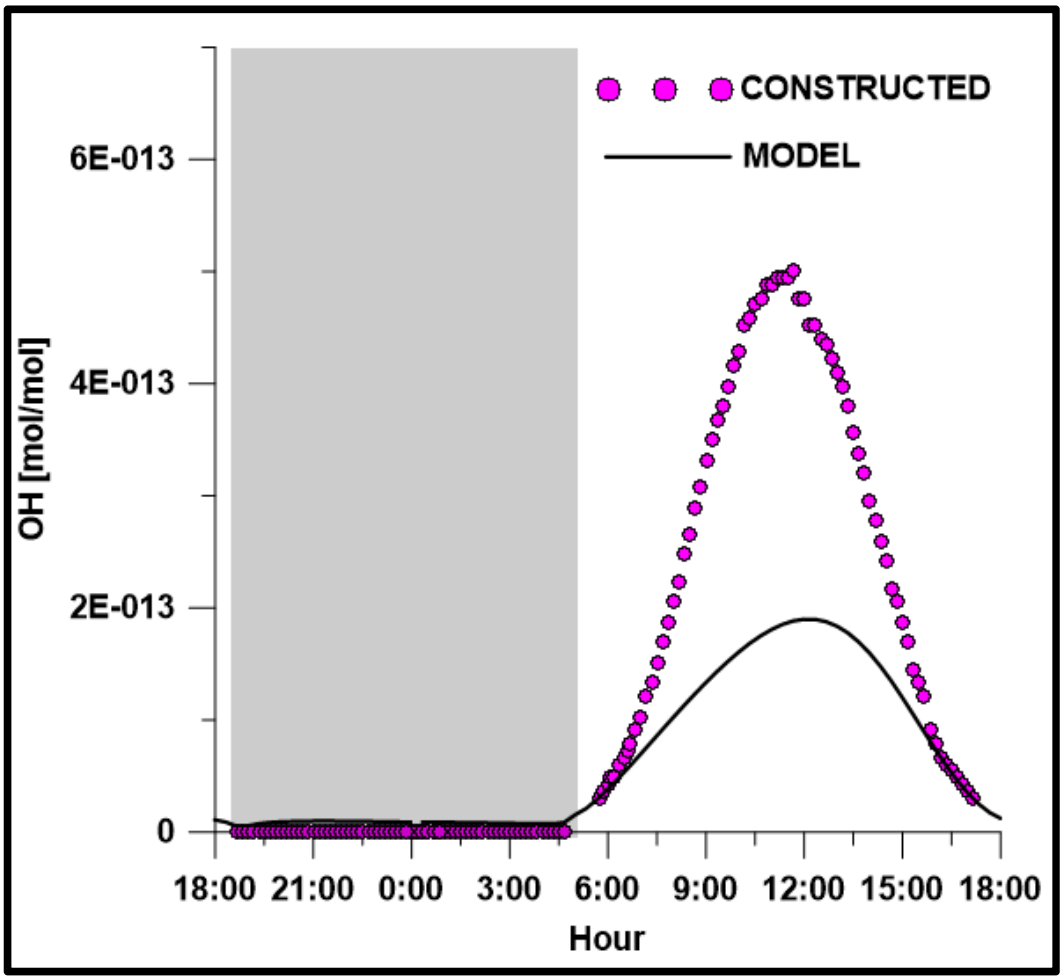

Figure S5. Comparison between constructed (see Sect. S1; pink dots) and simulated (black line) diurnal OH profiles. The shaded area represents nighttime.

Supplementary References

Ariya, P. A., Khalizov, A. and Gidas, A.: Reactions of gaseous mercury with atomic and molecular halogens: kinetics, product studies, and atmospheric implications, The Journal of Physical Chemistry A, 106, 7310-7320, 2002.

Calvert, J. G. and Lindberg, S. E.: A modeling study of the mechanism of the halogen–ozone–mercury homogeneous reactions in the troposphere during the polar spring, Atmos. Environ., 37, 4467-4481, 2003.

Hall, B.: The gas phase oxidation of elemental mercury by ozone, in: Mercury as a Global Pollutant, Springer, 301-315, 1995.

Hepler, L. G. and Olofsson, G.: Mercury. Thermodynamic properties, chemical equilibriums, and standard potentials, Chem. Rev., 75, 585-602, 1975.

Lin, C. and Pehkonen, S. O.: Aqueous free radical chemistry of mercury in the presence of iron oxides and ambient aerosol, Atmos. Environ., 31, 4125-4137, 1997.

Lin, C. and Pehkonen, S. O.: Aqueous phase reactions of mercury with free radicals and chlorine: implications for atmospheric mercury chemistry, Chemosphere, 38, 1253-1263, 1999.

Mason, R. P. and Sheu, G.: Role of the ocean in the global mercury cycle, Global Biogeochem. Cycles, 16, 40-1-40-14, 2002.

Munthe, J.: The aqueous oxidation of elemental mercury by ozone, Atmospheric Environment.Part A.General Topics, 26, 1461-1468, 1992.

Pal, B. and Ariya, P. A.: Gas-phase HO-initiated reactions of elemental mercury: kinetics, product studies, and atmospheric implications, Environ. Sci. Technol., 38, 5555-5566, 2004a.

Pal, B. and Ariya, P. A.: Studies of ozone initiated reactions of gaseous mercury: kinetics, product studies, and atmospheric implications, Physical Chemistry Chemical Physics, 6, 572-579, 2004b.

Pehkonen, S. O. and Lin, C.: Aqueous photochemistry of mercury with organic acids, J. Air Waste Manage. Assoc., 48, 144-150, 1998.

Pleuel, K. and Munthe, J.: Modelling the atmospheric mercury cycle-chemistry in fog droplets, Atmos. Environ., 29, 1441-1457, 1995.

Schroeder, W. H. and Munthe, J.: Atmospheric mercury—an overview, Atmos. Environ., 32, 809-822, 1998.

Shon, Z., Kim, K., Kim, M. and Lee, M.: Modeling study of reactive gaseous mercury in the urban air, Atmos. Environ., 39, 749-761, 2005.

Smith, S., Lee, J., Bloss, W., Johnson, G., Ingham, T. and Heard, D.: Concentrations of OH and HO 2 radicals during NAMBLEX: measurements and steady state analysis, Atmospheric Chemistry and Physics, 6, 1435-1453, 2006.

Sommar, J., Hallquist, M., Ljungström, E. and Lindqvist, O.: On the gas phase reactions between volatile biogenic mercury species and the nitrate radical, J. Atmos. Chem., 27, 233-247, 1997.

Sommar, J., Gårdfeldt, K., Strömberg, D. and Feng, X.: A kinetic study of the gas-phase reaction between the hydroxyl radical and atomic mercury, Atmos. Environ., 35, 3049-3054, 2001.

Stone, D., Whalley, L. K. and Heard, D. E.: Tropospheric OH and HO 2 radicals: field measurements and model comparisons, Chem. Soc. Rev., 41, 6348-6404, 2012.

Tokos, J. J., Hall, B., Calhoun, J. A. and Prestbo, E. M.: Homogeneous gas-phase reaction of Hg0 with H2O2, O3, CH3I, and (CH3) 2S: Implications for atmospheric Hg cycling, Atmos. Environ., 32, 823-827, 1998.

Van Loon, L., Mader, E. and Scott, S. L.: Reduction of the aqueous mercuric ion by sulfite: UV spectrum of HgSO3 and its intramolecular redox reaction, The Journal of Physical Chemistry A, 104, 1621-1626, 2000.

Van Loon, L. L., Mader, E. A. and Scott, S. L.: Sulfite stabilization and reduction of the aqueous mercuric ion: kinetic determination of sequential formation constants, The Journal of Physical Chemistry A, 105, 3190-3195, 2001.

von Glasow, R., Sander, R., Bott, A. and Crutzen, P. J.: Modeling halogen chemistry in the marine boundary layer 1. Cloud-free MBL, Journal of Geophysical Research: Atmospheres (1984–2012), 107, ACH 9-1-ACH 9-16, 2002.

Wang, Z. and Pehkonen, S. O.: Oxidation of elemental mercury by aqueous bromine: atmospheric implications, Atmos. Environ., 38, 3675-3688, 2004.

Xie, Z., Sander, R., Pöschl, U. and Slemr, F.: Simulation of atmospheric mercury depletion events (AMDEs) during polar springtime using the MECCA box model, Atmospheric Chemistry and Physics, 8, 7165-7180, 2008.

Zhang, L., Wright, L. P. and Blanchard, P.: A review of current knowledge concerning dry deposition of atmospheric mercury, Atmos. Environ., 43, 5853-5864, 2009.